# 3D KMC simulations of crater growth during the reduction of oxide nanoislands on metal surfaces

Liang Li, Guangwen Zhou *

Department of Mechanical Engineering and Multidisciplinary Program in Materials Science and Engineering, State University of New York, Binghamton, United States

## ARTICLE INFO

## ABSTRACT

The homoepitaxial growth of Cu nanocraters induced by thermal reduction of $Cu_2O$ nanoislands on $Cu(100)$ surfaces is simulated using a three-dimensional (3D) kinetic Monte Carlo (KMC) model by incorporating surface diffusion, attachment and detachment Cu adatoms dislodged from reducing $Cu_2O$ islands. The craters are observed to grow continuously in rim height and rim slopes while remaining relatively constant in rim width in the course of the oxide decomposition. Such a growth behavior is attributed to the climbing uphill of Cu adatoms released from the perimeter of the reducing $Cu_2O$ island at the crater bottom. The observed decay of the rim height and slopes after completion of the reduction of oxide islands suggests that these surface craters are thermodynamically unstable at high temperatures.

© 2010 Elsevier B.V. All rights reserved.

## 1. Introduction

The reduction of metal oxides plays a crucial role for many practical applications. In heterogeneous catalysis, metal oxides are used as active catalysts, metal supports, and promoter additives. Pretreatment and regeneration of the catalytic systems and actual catalytic reactions can take place in a reducing environment. Pure stoichiometric oxides usually do not exhibit high catalytic activity and oxide reduction is frequently employed to modify their adsorption properties [1–7]. Oxide reduction is also frequently involved in hydrometallurgical processes for recovering pure metals from their native oxides [8]. Other processes of oxide reduction include fabrication of electronic devices, magnetic memory components and active/passive solar materials systems [9–14].

Traditionally, the reduction process of metal oxides has been described using phenomenological kinetic models. e.g., "nucleation and growth model" and "interface model" [4,6,7,15,16]. As schematically shown in Fig. 1(a), in the "nucleation and growth model", generation of small nuclei of the reduced phase occurs on the oxide surface and the reaction interface increases until growing nuclei coalesce and then decreases. In the second case the entire surface of the oxide particle is covered with a thin layer of the solid product very soon after contacting the reducing gas (Fig. 1b). The reaction boundary advances inward uniformly as the reaction proceeds, resulting in a spherical core of the oxide that shrinks with time. This is known as the *interface-controlled* model. The *interface-controlled* model is an extreme case of the *nucleation-controlled* model in that it can be

assumed that the number density of small grains of reduced oxide is so large that boundaries of the grains overlap soon after the reaction.

Although these phenomenological kinetic models are found useful in the description of the reduction process of oxide single crystals and oxide powders [5–7,17–19], recent studies showed that they are not applicable to the reduction process of oxide nanoislands on metal surfaces. Using *in situ* transmission electron microscopy and atomic force microscopy techniques, it was shown recently that the thermal reduction of $Cu_2O$ islands on $Cu(100)$ surfaces results in the dislodgement of Cu atoms from reducing oxide islands, leading to the homoepitaxial growth of the reduced phase (e.g. Cu) on the substrate surface surrounding the oxide islands rather than on the parent oxide (Fig. 1c) [20,21]. This reduction phenomenon is fundamentally different from the assumption by the phenomenological kinetic models as shown in Fig. 1(a, b). In this work we develop a three-dimensional (3D) kinetic Monte Carlo method by incorporating surface diffusion and attachment/detachment of adatoms to study the growth of Cu craters during reduction of $Cu_2O$ nanoislands on $Cu(100)$ surfaces. Besides reproducing the experimentally observed crater morphologies, our simulations also reveal that these surface craters are thermodynamically unstable at the high temperatures and the detachment of Cu atoms from the crater rim can lead to the decay of the crater rim after the completion of the oxide reduction.

## 2. Model and method

Our simulation system is $Cu_2O$ nanoislands on a $Cu(100)$ surface. The thermal reduction of $Cu_2O$ is described by $Cu_2O(s) \rightarrow 2Cu + \frac{1}{2}O_2(g)$, where the oxygen gas is considered to desorb completely from the Cu surface due to the high reduction temperatures (~800 °C) and the small solubility of oxygen in bulk copper [22,23]. As shown in Fig. 1c,

* Corresponding author.
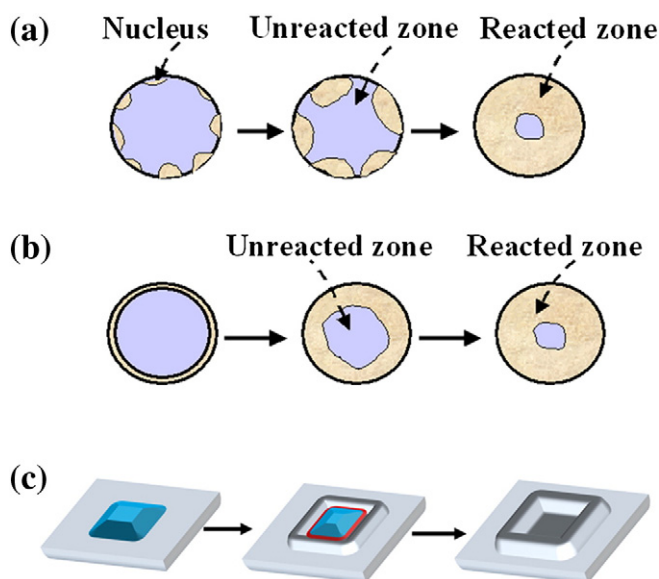E-mail address: gzhou@binghamton.edu (G. Zhou).

**Fig. 1.** Comparison of the previously proposed oxide reduction models – (a) "nucleation and growth" model; (b) "interface" model – to (c) our proposed "perimeter" model for the reduction of oxide nanoislands on a metal surface, where the perimeter is the contact line (marked by the red line) of the island bottom with the metal substrate, and oxide dissociation occurs preferentially along this perimeter.

the adjacent Cu substrate provides a perfect template for homo-epitaxial growth of released Cu adatoms (i.e., Cu atoms are more strongly bound to the Cu substrate than the $Cu_2O$ island under the reduction environments). Because the perimeter of the oxide island is the conjunction line between the oxide phase and metal substrate, Cu atoms in the oxide phase are released preferentially along the island perimeter and then diffuse over the Cu substrate. Since the rate of the oxide reduction is fast at a high temperature (~800 °C), Cu adatoms build up and form three-dimensional mounds (i.e., crater) surrounding the reducing $Cu_2O$ island. On the other hand, Cu atoms may also detach from the growing Cu craters at high temperatures. Therefore, the size evolution of the Cu crater would be determined by the difference between how fast copper adatoms are added onto the growing crater and how fast the Cu crater thermally smoothes via atom detachment from the growing crater rim.

The kinetic Monte Carlo model used in our simulations is a full-diffusion bond-counting model including the nearest-neighbor interactions. The mobility of Cu adatoms released from the reducing oxide island obeys an Arrhenius law and the surface migration can be modeled as a nearest-neighbor hopping process at the rate, $k(E,T) = v_0 \exp(-E/k_BT)$, where E is the coordination-number dependent hopping barrier for surface diffusion, T is the reduction temperature, and $k_B$ is Boltzmann's constant. The attempt frequency $v_0$ is $v_0 = k_BT/h = 4.2 \times 10^{10} T$, with h Plank's constant, and T given in degrees Kelvin. The hopping barrier E depends on the local environment of an atom. A common assumption is that the barrier for motion in any direction is proportional to the current number of nearest-neighbor bonds while taking into account the difference between adatom–substrate bonds and adatom–adatom bonds [24–27]. Therefore, E is composed of a substrate term $E_S$, a contribution $E_N$ from each in-plane nearest neighbor, and the step-edge barrier $E_B$ if a step is present, i.e., $E = E_S + nE_N + (m_i - m_f)E_B$, where n is the number of in-plane nearest neighbors before the hop, $m_i$ and $m_f$ are the number of the next-nearest neighbors in the planes beneath and above the hopping atom before ($m_i$) and after ($m_f$) a hop, respectively. The binding energy of an adatom at the surface can be described by the first two terms (i.e. $E_S + nE_N$, which depends only on n. This implies that the detailed balance is satisfied and the thermodynamic equilibrium can be established. The step-edge barrier $E_B$ has a nonzero value only if $m_i > m_f$.

The presence of the step-edge barrier $E_B$ depends on a hop direction, and the effect of this energy barrier is to make the motion of an adatom down a step edge less favorable than motion on the terrace [28,29]. The number of the next-nearest neighbors both before and after the hop has to be considered in order to detect a step.

The effect of surface sublimation is neglected in our model. This is because we have observed experimentally Cu crater formation under a wide range of temperature and vacuum conditions (i.e., $T \geq 650$ °C and the vacuum from ~$4 \times 10^{-6}$ Torr to ~$2 \times 10^{-8}$ Torr), some of which have negligible Cu sublimation. This suggests that Cu sublimation is not a vital process in the formation of surface craters. Another process neglected in our simulations is the effect of vacancy diffusion. Vacancy diffusion was shown to have a significant effect on surface evolution if vacancies and adatoms have comparable formation energies and diffusion constants [30]. In our case, Cu crater growth happens as a result of the spontaneous decomposition of $Cu_2O$ islands, through which Cu adatoms are supplied without additional formation energy. Such a process of Cu crater growth is similar to deposition, where the Cu adatoms are supplied from a confined surface (i.e. a $Cu_2O$ island) at the substrate surface. The decomposition of a $Cu_2O$ island leads to a locally high concentration of Cu adatoms (above the equilibrium concentration of surface atoms) for nucleation and growth of the Cu hill surrounding the reducing oxide island. In contrast, vacancy transport will require generation of a large amount of vacancies on the surface and this would be not kinetically favorable in comparison to the adatom process. The effect of vacancy diffusion is therefore not included in the simulations. Our simulations were carried on a $250 \times 250 \times 40$ matrix. The oxide reduction is initiated by random dislodgement of Cu atoms from the perimeter of a $Cu_2O$ pyramid. The model parameters used are $E_S = 0.49$ eV [31], $E_N = 0.24$ eV [31], and $E_B = 0.27$ eV [32,33] and given in Table 1, as obtained from the self-diffusion of Cu adatoms on terraces and at edges and steps.

## 3. Results and discussion

In the simulations, the reduction stage is determined by the total number of Cu atoms released from a reducing $Cu_2O$ island. We monitor the morphological evolution of the reaction product at different stages and surface cratering is observed from our 3D KMC simulations. Fig. 2(a–c) shows snapshots of the crater morphology during reduction of a square $Cu_2O$ pyramid at T = 800 °C. As it can be seen, reduction of the oxide island results in build-up of Cu adatoms on the substrate surface adjacent to the reducing $Cu_2O$ island, rather than filling up on the oxide surface, which is consistent with our experimental observation [20,21]. Complete reduction of the oxide pyramid leads to formation of a crater on the Cu surfaces. The crater base is observed to take a shape similar to the oxide pyramid prior to its reduction. For comparison purpose, Fig. 2(d) shows an experimental atomic force microscopy (AFM) image of the surface crater obtained from thermal reduction of an oxide pyramid at 800 °C (the AFM imaging was performed at room temperature). Fig. 2(e, f) are the line profiles from the simulated crater and the experimental AFM images, which reveal comparable surface morphology and slopes between the simulation results and experimental observation.

**Table 1**
Energy barriers ($E = E_S + nE_N + (m_i - m_f) E_B$) in eV used in the kMC simulations. The details of the atomic processes are shown in Fig. 2.

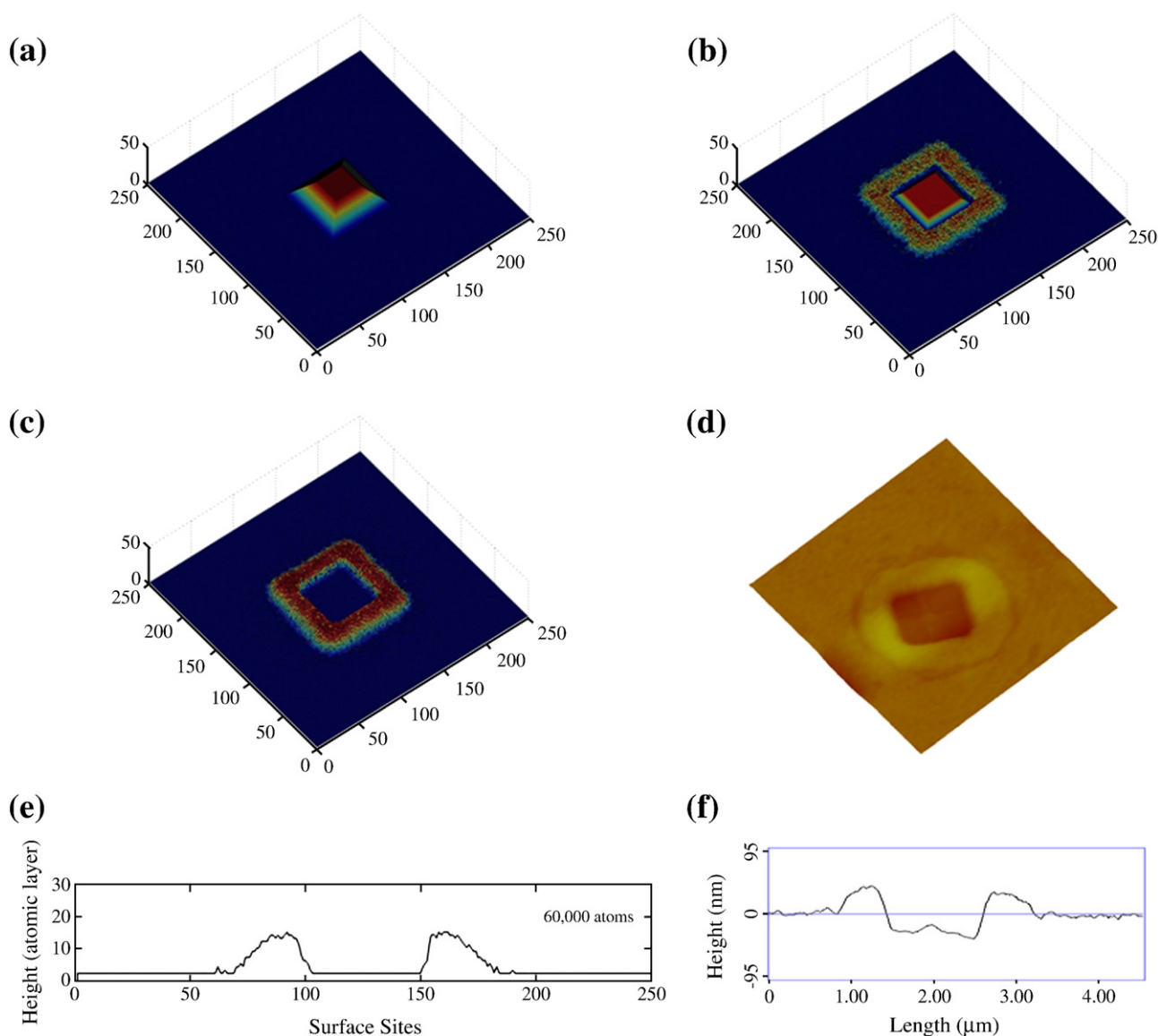|  | eV |
| --- | --- |
| Terrace diffusion ($E_S$) | 0.49 |
| Diffusion away from a step ($E_S + E_N$) | 0.73 |
| Diffusion to a step edge ($E_S + E_B$) | 0.76 |
| Descent at a step edge ($E_S + E_N$) | 0.73 |
| Ascent at a step ($E_S + E_N + E_B$) | 1 |

Fig. 2. Snapshots from our 3D KMC simulations of the reduction of a square Cu$_2$O pyramid on a Cu(100) surface: (a) the oxide island prior to its reduction; (b) 30,000 Cu atoms are dislodged from the reducing island; (c) after the complete reduction of the oxide island (total 60,000 Cu atoms); (d) an experimental AFM image of the surface crater obtained by thermal reduction of a Cu$_2$O pyramid at 800 °C under vacuum (4.5×4.5 μm$^2$, z range: 0.2 μm); (e) line scan profile from the simulated crater in (c) and (f) line scan profile from the AFM image in (d).

We then examine the morphological evolution of the surface craters obtained from our 3D KMC simulations. Fig. 3 shows snapshots of the cross-sectional view of the crater at its different growth stages. Several distinct features can be noticed. First, the height of the crater rim increases continuously in the course of the oxide reduction (Fig. 4a), while the rim width remains relatively constant. Secondly, both the inner and outer sidewalls of the crater rim show the growth instability, as illustrated by the thickness dependence of the rim slopes. Fig. 4b reveals that the inner slope is steeper than the outer slope at each growth stage, which is consistent with the experimental observation as shown in Fig. 2(f), where the inner slope is larger than the outer slope by ~11°. Fig. 4b also indicates that both the inner and outer slopes grow with continued crater growth.

One of the most intriguing features is the formation of the crater rim, which can be more than ten atomic layers thick. Formation of the crater rims should be kinetic in nature in the present homoepitaxial system involving attachment of adatoms from the reducing Cu$_2$O island and detachment of Cu atoms out of the growing Cu crater. The large heights of the crater rim suggest that the rate of the attachment

of Cu adatoms released from the reducing Cu$_2$O island is much faster than the rate of detachment of Cu atoms from the crater rim. Indeed, the activation energy for an atom to leave a stable site (i.e., the site with the low free-energy configuration) by breaking neighboring bonds would be higher than to find a stable site via surface diffusion.

Besides the unequal rates of attachment and detachment of Cu atoms, growth of the large crater rims also involves transfer of Cu atoms from the reducing Cu$_2$O island to the surrounding Cu crater. It has been shown previously that the perimeter of an oxide pyramid, as marked by the red line in Fig. 1(c), is the kinetically favorable sites for oxide decomposition [20]. Therefore, homoepitaxial growth of the crater rim (i.e., the rim thickening) must call for upward diffusion of Cu adatoms from the crater bottom onto the top of the growing rim along the inner wall. Such a process of adatom ascending is active whenever steps are present [34,35], and it becomes more efficient as increasing the substrate temperature (here T = 800 °C for the oxide reduction). This temperature effect can also be inferred from KMC simulations at different temperatures of the oxide reduction. Fig. 5 shows the rim slopes of the craters formed from the reduction of a
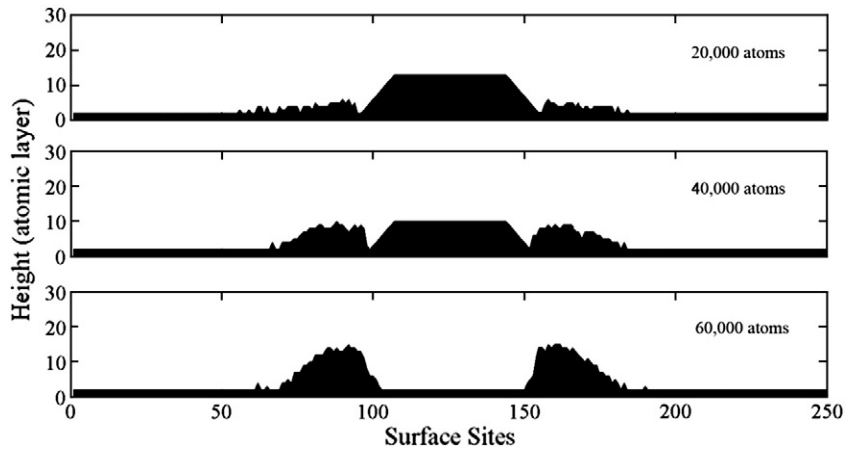
**Fig. 3.** Snapshots of cross-sectional views of a crater at its different growth stages in the course of oxide reduction, from which the slopes of the inner and outer sidewalls of the crater rim as well as the rim heights can be measured.

square Cu₂O pyramid at the different temperatures. Both the inner and outer slopes become steeper as increasing the reduction temperature from 600 °C to 800 °C, suggesting an enhanced upward diffusion of adatoms at the higher temperatures. However, it is noted from Fig. 5 that there is a slight downward trend in the magnitude of the rim slopes for the temperature at 900 °C. The slight decrease in the slopes is caused by the enhanced detachment of Cu atoms from the

growing crater at 900 °C, which causes thermal smoothing of the crater rim (this effect is shown later).

Another striking feature observed from the simulations is the asymmetrical slope evolution of the slopes of inner and outer walls of the crater rim. The inner wall is steeper than the outer sidewall, implying different kinetic processes along the two sidewalls. The cause for the wall steepening as well as for the relatively constant rim width is
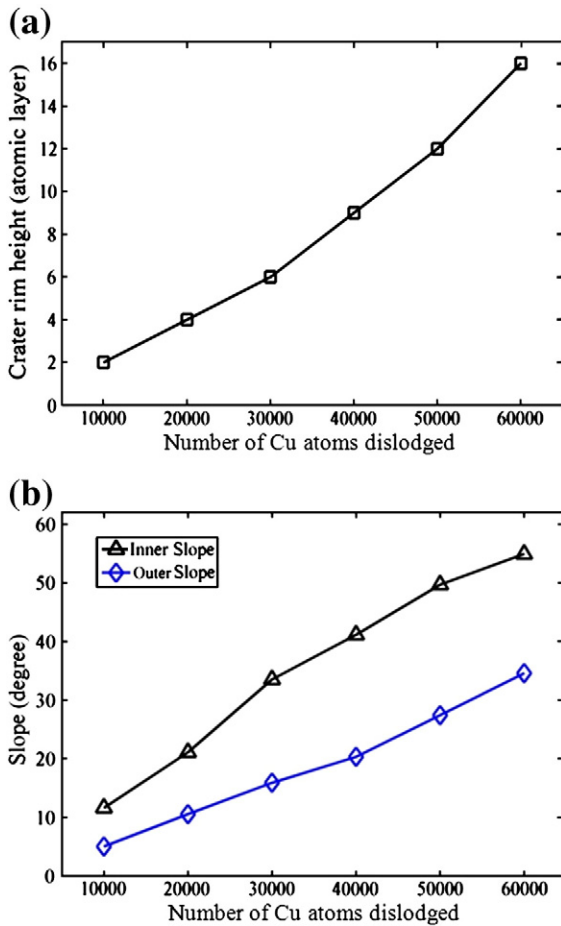


**Fig. 4.** (a) Evolution of the crater rim height as a function of the number of Cu adatoms dislodged in the course of the oxide reduction; (b) evolution of the slopes of the inner and outer sidewalls of the crater rim as a function of Cu adatoms dislodged from the reducing Cu₂O island.
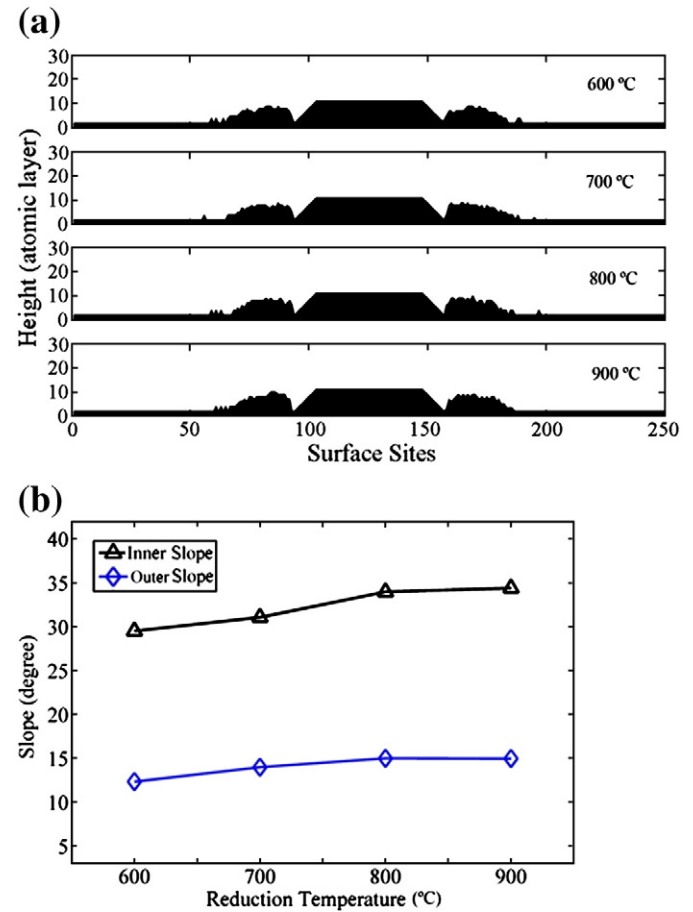
**Fig. 5.** (a) Cross-sectional views of the craters during reduction of a square Cu₂O pyramid (total 30,000 Cu atoms) at different temperatures; (b) Temperature dependence of the slopes of the inner and outer sidewalls of the crater rim as measured from the KMC simulations at the different temperatures.
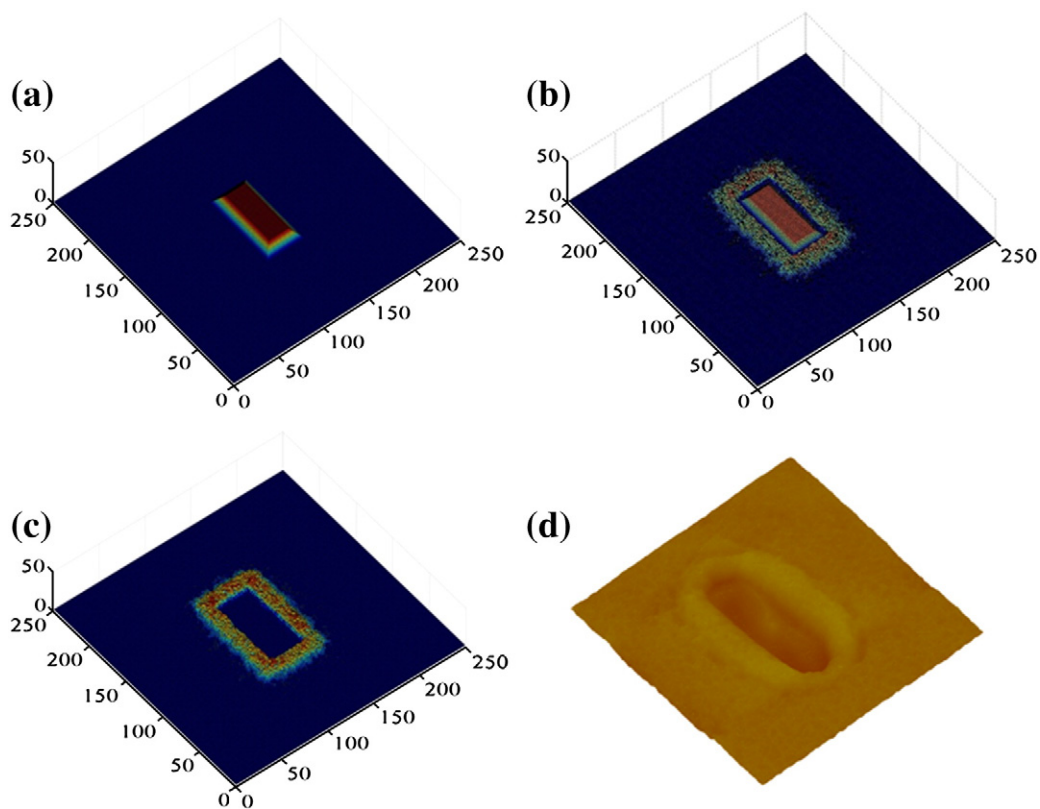
**Fig. 6.** KMC simulations of the growth of a rectangular crater (total 60,000 Cu atoms), (a) the island prior to its reduction, (b) 30,000 Cu atoms dislodged from the reducing island, and (c) complete reduction of the oxide island; (d) experimental AFM image of a rectangular crater (5×5 μm², z range: 0.15 μm).
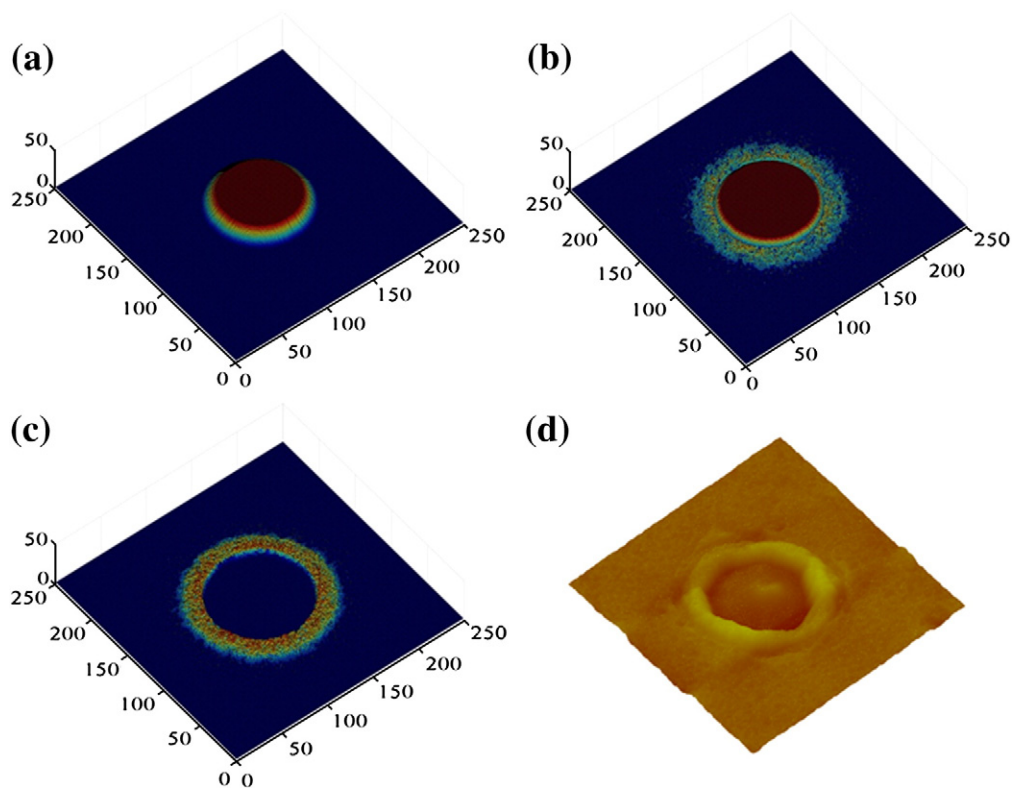


**Fig. 7.** KMC simulations of the growth of a round-shape crater (total 60,000 Cu atoms), (a) the island prior to its reduction, (b) 30,000 Cu atoms dislodged from the reducing island, and (c) complete reduction of the oxide island; (d) experimental AFM image of a round-shape crater (5×5 μm², z range: 0.15 μm).
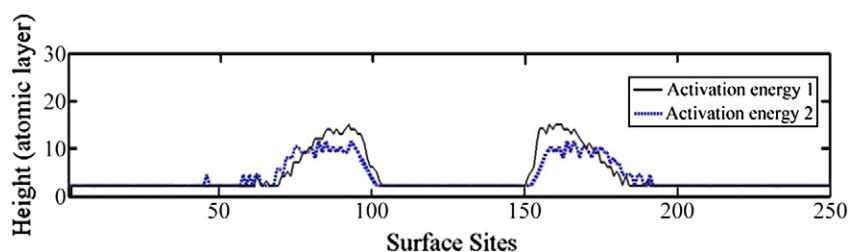
**Fig. 8.** Surface profiles of the simulated craters using different activation energy values, where the activation energy set 1 is given in Table 1, and the activation energy set 2 corresponds to half the value of the energies in Table 1.

related to the step-edge barrier ($E_B$) that hinders the rim lateral growth by preventing adatoms to diffuse over a step edge from an upper to a lower terrace. The evolution of the outer wall is largely determined by the adatom descending while the growth of the inner wall depends on both adatom descending and ascending. The larger slope for the inner sidewall is caused by the net uphill diffusion of Cu adatoms along the inner wall.

Our 3D KMC simulations of crater growth are based on the homoepitaxial growth of Cu adatoms dislodged from the perimeter of a decomposing Cu$_2$O island at the cater bottom. Homoepitaxy has conventionally been modeled as the processes of adatoms "raining" down onto a growing surface and pyramid-like mound morphologies are usually observed. As deposition continues, the mounds grow bigger and steeper (i.e., unstable), and may ultimately reach a steady state characterized by an approximately constant mound angle caused either by the balance between an uphill diffusion flux of adatoms formed by the edge-step barrier [28,29,36,37] and a downhill flux caused by the "downward funneling" effect [38–40] or by the formation of some specific side facets that favor upward diffusion of adatoms [32,34,41,42]. However, growth of the crater rims by Cu homoepitaxy during the reduction of Cu$_2$O islands in our system does not involve deposition of adatoms "raining" down onto the entire growing surface; alternatively, the adatoms are supplied from a confined Cu source at the substrate

surface. Therefore, in spite of the larger activation energy required for adatom ascending, there is still a net uphill current of Cu adatoms climbing along the inner wall, leading to the thickening of the crater rim. These unusual kinetic processes lead to the observed growth features such as the asymmetrical evolution of the slopes of the inner and outer sidewalls of the crater rims. Such asymmetrical growth kinetics would not be expected for conventional "raining-down" deposition processes [26,27,43–45].

It can be noted from Fig. 2 that the crater shape is correlated with the morphology of the oxide island. To examine if this is the case for other island shapes, we simulated the growth of craters from reduction of rectangular and round-shaped Cu$_2$O pyramids. As shown in Fig. 6(a–c), reduction of a rectangular oxide pyramid results in formation of a crater with a rectangular base. For comparison, an experimental AFM image of the surface crater obtained by reduction of rectangular Cu$_2$O pyramids is given in Fig. 6(d). Fig. 7(a–c) shows snapshots of the reduction of an oxide pyramid with a round base and Fig. 7(d) is an experimental AFM image of the surface crater obtained from the reduction of a round Cu$_2$O pyramid. The excellent agreement in the crater morphologies between the simulations and experiments further suggests that our model has captured correctly the basic atomic processes governing the crater growth, i.e., Cu atoms are released along the perimeter of the oxide island, where they start to
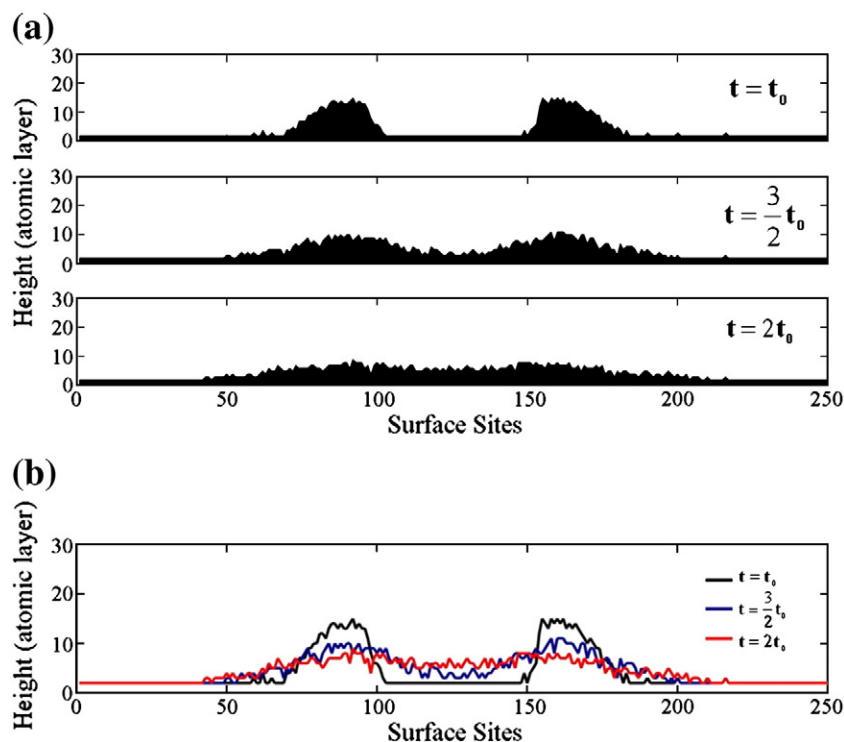


**Fig. 9.** (a) Cross-sectional view of the morphological evolution of a crater annealed at 800 °C, where $t_0$ corresponds to the time required for complete reduction of an oxide island with 60,000 Cu atoms; $\frac{3}{2}t_0$ and $2t_0$ are the annealing time followed after the completion of reduction of the oxide island; (b) comparison of surface profiles of the crater at the different annealing times, the crater decay can be seen from the shrinking rim height and slopes.

bind pure Cu and form 3D mounds via adatom ascending. Since the shape of oxide islands can be controlled by adjusting the oxidation conditions (i.e., oxidation temperature, substrate orientation, etc.) of the Cu substrates [46–48], such a correlation allows for the control of the crater shape via manipulating the oxidation/reduction conditions.

Although the results of our simulations agree well with the experimental observations of crater morphologies, a pertinent question is whether the phenomena revealed by the simulations depend on the details of the model, i.e., how general the observed phenomena might be. Therefore, we simulated the crater growth using different activation energies for adatom surface diffusion and attachment/detachment. Fig. 8 shows simulated craters with the use of two different sets of the activation energies, where the energies of set I are the same given in Table 1, and set II corresponds to half the value of the energies in Table 1. It can be seen that the crater formed with the activation energy set II has smaller rim heights and slopes but a larger rim width. By comparing the crater structure (e.g., rim height and slopes) between the simulations and experimental AFM images, we note that the simulations using the activation energies of set I give a better match with the experiments. The observation suggests that cratering may be a general phenomenon accompanying with decomposition of oxide nanoislands, but the cater structure would depend on the particular materials properties (bonding strength, diffusion barrier, etc.). Craters formed from different metal/oxide systems may have different topological features such as ratios of rim height/width and outer/inner slopes.

The observed crater growth shown above is from simulations which are terminated once a $Cu_2O$ island is completely decomposed. This is consistent with our experiment observation, where the AFM imaging was performed with the thermally reduced Cu surface which was cooled down quickly to room temperature after the oxide is completely decomposed at the high temperatures (the size evolution of oxide islands can be monitored by *in situ* TEM during the oxide reduction [20]). However, if the effect of surface energy on surface morphology evolution is considered, formation of the crater rim with large sidewall slopes (i.e., the formation of high-index facets or rough surface) is thermodynamically unfavorable due to the higher surface energies. Therefore, craters would evolve to lower surface energies if given enough annealing time at the high temperature. To test this speculation, we run the simulations continuously after the oxide reduction is completed. Fig. 9 shows the morphological evolution of a crater annealed at 800 °C, the thermal smoothing of the crater rim can be observed from continued shrinkage of the rim height and slopes. The decay of the crater rim is caused by the net detachment of Cu atoms from the crater rim after the complete reduction of the $Cu_2O$ island (i.e., the crater growth would stop since there are no new Cu adatoms available to sustain the growth).

Our model is a full-diffusion bond-counting model which includes the nearest-neighbor atom interactions. Surface energy is a property depending on the number of dangling bonds at the surface, and this effect is taken into account in our model from the NN dependent diffusion barrier. For instance, in the absence of an external flux (in our case, the external flux is the flux of Cu adatoms released from a reducing $Cu_2O$ island), this nearest-neighbor dependent barrier would drive the system to its lowest free-energy configuration. This effect is seen from the decay of Cu craters after the oxide islands are completely reduced.

The above observations suggest that the morphological evolution of Cu craters would depend on the annealing time and the initial $Cu_2O$ island size. We examined the formation of craters during the reduction of $Cu_2O$ islands with different island sizes on the same Cu surface, and the simulation result is shown in Fig. 10(a–b). With the continued annealing the small crater grown from reduction of a small $Cu_2O$ island has changed from growing to decay whereas the large ones are still growing because of the longer time needed for completely decomposing the large $Cu_2O$ islands. Crater coalescence
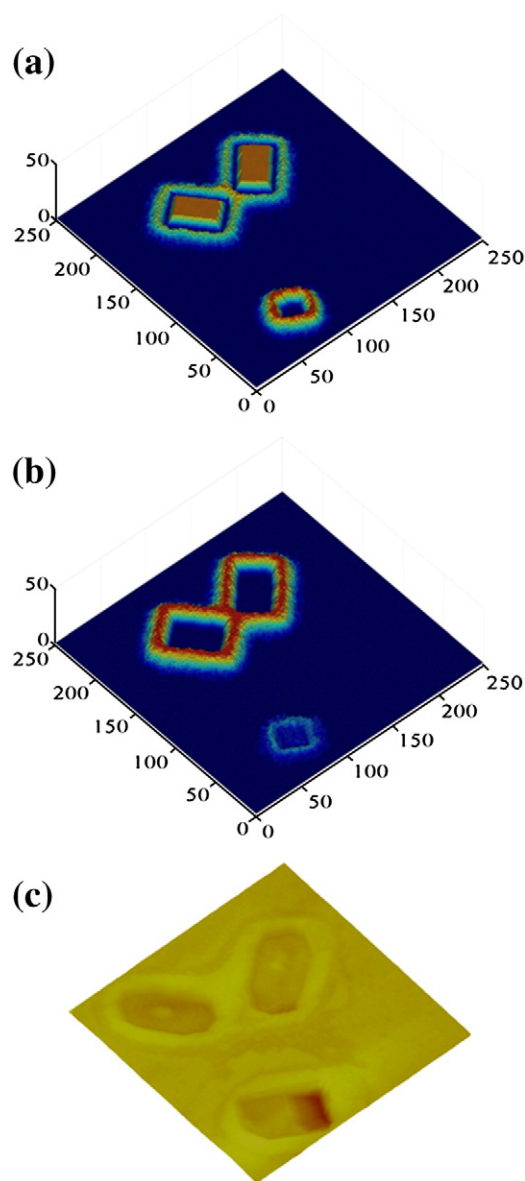


**Fig. 10.** KMC simulations of the morphological evolution of craters during the reduction of $Cu_2O$ pyramids with different island sizes: (a) the reaction stage corresponding to the complete reduction of the small $Cu_2O$ island; (b) with continued annealing, the small crater is shrinking while the large craters associated with large $Cu_2O$ islands are still growing; and (c) an experimental AFM image ($6.5 \times 6.5$ μm², z range: 0.4 μm) of the surface craters obtained by the complete reduction of $Cu_2O$ pyramids with different island sizes.

is also observed between the two large islands due to their small island spacing. Such a size-dependent crater growth/decay behavior is expected to lead to a relatively uniform size distribution of survived craters after the complete reduction of all the oxide islands. For comparison, an experimental AFM image obtained from the complete reduction of $Cu_2O$ islands with different island sizes is given in Fig. 10c, where only larger craters are visible.

## 4. Conclusions

We have developed a 3D KMC approach to simulate surface cratering during the reduction of $Cu_2O$ islands on Cu(100) surfaces. Both the rim height and the slopes are observed to grow while the rim width remaining relatively constant in the course of the oxide reduction. These growth features can be attributed the net uphill diffusion of Cu adatom along the inner wall of the crater rim at the

high temperatures. The observed crater decay after the completion of the oxide decomposition suggests that these surface craters are thermodynamically unstable structures at the high temperatures. The size-dependent cater growth and decay is observed, resulting in a relatively uniform size distribution of survived Cu craters. We expect such a process of crater growth can be further exploited for creating novel structures at metal surfaces via the mass reorganization during reduction of oxide nanoislands.

## Acknowledgements

## References

[1] V.E. Henrich, P.A. Cox, The Surface Science of Metal Oxides, Cambridge University Press, Cambridge, 1994.
[2] A. Bouzoubaa, A. Markovits, M. Calatayud, C. Minot, Surf. Sci. 583 (2005) 107.
[3] V.A. Bondzie, P.H. Kleban, D.J. Dwyer, Surf. Sci. 465 (2000) 266.
[4] H.H. Kung, Transition Metal Oxides: Surface Chemistry and Catalysis, Elsevier, New York, 1989.
[5] J.Y. Kim, J.A. Rodriguez, J.C. Hanson, A.I. Frenkel, P.L. Lee, J. Am. Chem. Soc. 125 (2003) 10684.
[6] J.A. Rodriguez, J.Y. Kim, J.C. Hanson, M. Perez, A.I. Frenkel, Catal. Lett. 85 (2003) 247.
[7] J.A. Rodriguez, J.C. Hanson, A.I. Frenkel, J.Y. Kim, M. Perez, J. Am. Chem. Soc. 124 (2002) 346.
[8] K.M. Sista, C.M. Sliepcevich, Metall. Trans. B 12 (1981) 565.
[9] Y.Z. Hu, R. Sharangpani, S.P. Tay, J. Electrochem. Soc. 148 (2001) G669.
[10] S.Y. Lee, N. Mettlach, N. Nguyen, Y.M. Sun, J.M. White, Appl. Surf. Sci. 206 (2003) 102.
[11] R. Govindaraj, C.S. Sundar, R. Kesavamoorthy, J. Appl. Phys. 100 (2006) 084318.
[12] F. Irrera, G. Puzzilli, D. Caputo, Microelectron. Reliab. 45 (2005) 853.
[13] J. Li, J.W. Mayer, K.N. Tu, Phys. Rev. B 45 (1992) 5683.
[14] P.D. Kirsch, J.G. Ekerdt, J. Appl. Phys. 90 (2001) 4256.
[15] B. Delmon, in: G. Ertl, H. Knozinger, J. Weitkamp (Eds.), Handbook of Heterogeneous Catalysis, Wiley-VCH, New York, 1997, p. 264.
[16] C. H. Bamford, C. F. H. Tipper, and R. G. Compton, (Elsevier, New York, 1984), Vol. 21.
[17] J.G. Chen, D.A. Fischer, J.H. Hardenbergh, R.B. Hall, Surf. Sci. 279 (1992) 13.
[18] R.P. Furstenau, G. McDougall, M.A. Langell, Surf. Sci. 150 (1985) 55.
[19] T. Ressler, R.E. Jentoft, J. Wienold, M.M. Gunter, O. Timpe, J. Phys. Chem. B 104 (2000) 6360.
[20] G.W. Zhou, J.C. Yang, Phys. Rev. Lett. 93 (2004) 226101.
[21] G.W. Zhou, W.Y. Dai, J.C. Yang, Phys. Rev. B 77 (2008) 245427.
[22] M. Hansen, Constitution of Binary Alloys, McGraw-Hill, NY, 1958.
[23] R.L. Pastorek, R.A. Rapp, Trans. The Metall. Soc. AIME 245 (1969) 1711.
[24] C. Ratsch, A. Zangwill, P. Smilauer, D.D. Wedensky, Phys. Rev. Lett. 72 (1994) 3194.
[25] G.S. Bales, D.C. Chrzan, Phys. Rev. B 50 (1994) 6057.
[26] P. Smilauer, D.D. Vvedensky, Phys. Rev. B 52 (1995) 14263.
[27] P. Smilauer, M.R. Wilby, D.D. Vvedensky, Phys. Rev. B 47 (1993) 4119.
[28] G. Ehrlich, F. Hudda, J. Chem. Phys. 44 (1966) 1039.
[29] R.L. Schwoebel, E.J. Shipsey, J. Appl. Phys. 37 (1966) 3682.
[30] J.B. Hannon, C. Klunker, M. Giesen, H. Ibach, N.C. Bartelt, J.C. Hamilton, Phys. Rev. Lett. 79 (1997) 2506.
[31] G. Boisvert, L.J. Lewis, Phys. Rev. B 56 (1997) 7643.
[32] W.G. Zhu, F. Buatier de Mongeot, U. Valbusa, E.G. Wang, Z.Y. Zhang, Phys. Rev. Lett. 92 (2004) 106102.
[33] The adatom ascending barrier at a monatomic-layer high step on Cu(100) surface is not readily available in the literature. Reference [24] gives an energy barrier of ~0.8 eV for adatom ascending on a Cu(110) surface. Since Cu(100) surface has a more compact structure than Cu(110), we therefore use a larger activation energy barrier, $E_S + E_N + E_B = 1.$eV for adatom ascending at a monatomic step on Cu (100) surface, which produces a good agreement with the experimental observation.
[34] F. Buatier de Mongeot, W.G. Zhu, A. Molle, R. Buzio, C. Boragno, U. Valbusa, E.G. Wang, Z.Y. Zhang, Phys. Rev. Lett. 91 (2003) 016102.
[35] P.F. Zhang, X.P. Zheng, S.P. Wu, J. Liu, D.Y. He, Vacuum 72 (2004) 405.
[36] S.C. Wang, G. Ehrlich, Phys. Rev. Lett. 70 (1993) 41.
[37] J.G. Amar, F. Family, Phys. Rev. Lett. 77 (1996) 4584.
[38] M.C. Bartelt, J.W. Evans, Phys. Rev. Lett. 75 (1995) 4250.
[39] J.W. Evans, P.A. Thiel, M.C. Bartelt, Surf. Sci. Rep. 61 (2006) 1.
[40] J.W. Evans, D.E. Sanders, P.A. Thiel, A.E. DePristo, Phys. Rev. B 41 (1990) 5410.
[41] H.L. Yang, Q. Sun, Z.Y. Zhang, Y. Jia, Phys. Rev. B 76 (2007) 115417.
[42] K. Fichthorn, M. Scheffler, Nature 429 (2004) 617.
[43] J.-K. Zuo, J.F. Wendelken, Phys. Rev. Lett. 78 (1997) 2791.
[44] S. van Dijken, L.C. Jorritsma, B. Poelsema, Phys. Rev. B 61 (2000) 14047.
[45] K.J. Caspersen, A.R. Layson, C.R. Stoldt, V. Fournee, P.A. Thiel, J.W. Evan, Phys. Rev. B 65 (2002) 193407.
[46] G.W. Zhou, J.C. Yang, Phys. Rev. Lett. 89 (2002) 106101.
[47] G.W. Zhou, J.C. Yang, Appl. Surf. Sci. 210 (2003) 165.
[48] G.W. Zhou, W.S. Slaughter, J.C. Yang, Phys. Rev. Lett. 94 (2005) 246101.